Journal of Power Sources 212 (2012) 154–160

Contents lists available at SciVerse ScienceDirect

Journal of Power Sources

journal homepage: www.elsevier.com/locate/jpowsour

# A Swiss-roll liquid–gas mixed-reactant fuel cell

Amin Aziznia [a,b], Colin W. Oloman [a,b,*], Előd L. Gyenge [a,b,*]

[a] Department of Chemical and Biological Engineering, The University of British Columbia, 2360 East Mall, Vancouver, BC, Canada V6T 1Z3
[b] Clean Energy Research Center (CERC), The University of British Columbia, 2360 East Mall, Vancouver, BC, Canada V6T 1Z3

ARTICLE INFO

*Article history:*
Received 5 March 2012
Received in revised form
24 March 2012
Accepted 26 March 2012
Available online 10 April 2012

*Keywords:*
Mixed reactant fuel cells
Direct borohydride fuel cells
Alkaline fuel cells
Electrochemical reactors

ABSTRACT

Fuel cells face challenges related to performance and cost that stem in part from constraints of the conventional plate-and-frame architecture in vogue since Volta's time. Here, we present for the first time a cylindrical Swiss-roll mixed-reactant fuel cell (SR-MRFC) that addresses some of these challenges by eliminating ion exchange membranes and flow-field plates, to provide a light, compact multi-cell stack. We demonstrate the monopolar and bipolar SR-MRFC for the borohydride-oxygen system, using a liquid/gas mixture of 1 M $NaBH_4$/2 M NaOH and $O_2$. A 3D anode with Pt/C (or PtRu/C) on carbon cloth was coupled with a gas-diffusion Ag/C (or $MnO_2$/C) cathode. At 323 K and atmospheric pressure, a peak power density of density of 1000 W $m^{-2}$ was achieved with good performance stability. The reactor concept presented here is applicable to a variety of alkaline or acid fuel cell systems.



## 1. Introduction

The commercialization of the fuel cell technology hinges on socio-economic 'pull' and technology 'push'. Both driving forces for technology adoption depend on a balance between performance and cost, respecting society, the economy and the environment. It is well-known that the capital and operating costs of fuel cell power systems must be reduced before they can be competitive with conventional energy conversion technologies. For this purpose, cheaper electrocatalysts and reactor designs are needed and fuel cell systems should be reduced in size, weight and complexity to meet the demands of many potential applications. Such objectives apply to the fuel cell stack and to the major subsystems making up the balance of plant. These technical and economic challenges are driving the development of unconventional fuel cell systems such as mixed-reactant fuel cells (MRFCs) [1].

In a conventional fuel cell, the fuel and oxidant flow in separate streams, kept apart by an ion conducting membrane that divides the cell into discreet anode and cathode chambers. The single-cells are stacked in series electric connection using bipolar flow-field plates that provide most of the stack weight and volume. The membrane and bipolar plates contribute respectively 15–68% and 10–25% to the stack cost, depending on the intended application and stack design [2]. By comparison to the conventional fuel cell, in an MRFC a mixture of fuel and oxidant flows through the cell as a single stream. Simplification of MRFCs systems is possible because they can operate without the gastight structures within the stack that are required for sealing, manifolding, and separate reactant delivery in conventional fuel cells. Corresponding simplifications may also be realized in the balance of plant. As a result, MRFCs could potentially provide relatively low cost fuel cell systems with high volumetric power density.

The MRFC is a relatively new configuration that has been described in the literature since the 1960's as a single electrochemical cell or stack of cells of various geometries in which a fuel/oxidant mixture flows to the anode and/or the cathode. Although the MRFC concept flouts reaction thermodynamics it is possible to contrive a practical mixed-reactant system based on the following three kinetic effects: a) avoiding spontaneous thermochemical reaction between the fuel and oxidant that may occur in the bulk reactant mixture or on catalyst surfaces, b) providing intrinsic kinetic selectivity of anode and/or cathode electrocatalysts to suppress mixed-potentials at the electrodes, and c) promoting selectivity of the electrodes for mass transfer of the fuel and oxidant respectively to the anode and the cathode. In reality these three mechanisms cannot be 100% effective, leading to thermochemical, electrochemical and/or mass transfer defects that lower the cell voltage, increase fuel consumption and decrease the energy efficiency of the MRFC. However, these deficiencies are balanced by potentially lower capital costs and higher power densities that could favor MRFC's over conventional systems in some applications.

* Corresponding authors. Department of Chemical and Biological Engineering, The University of British Columbia, 2360 East Mall, Vancouver, BC, Canada V6T 1Z3. Tel.: +1 604 822 3217; fax: +1 604 822 6003.
*E-mail addresses:* coloman@intergate.ca (C.W. Oloman), egyenge@chbe.ubc.ca, egyenge@chml.ubc.ca (E.L. Gyenge).

0378-7753/$ – see front matter © 2012 Elsevier B.V. All rights reserved.
doi:10.1016/j.jpowsour.2012.03.047

Since the 1960's, MRFCs have received attention in both low temperature (298–623 K) fuel cells [3–11] and high temperature (623–1273 K) solid oxide fuel cells (SOFCs) [12]. The low temperature MRFC research has been focused on three aspects: selective catalysts [4,5], mass transfer selectivity of the electrodes [3,6] and new fuel cell architectures [7–11]. Most of this research on low temperature MRFCs has been confined to conventional proton exchange membrane (PEM) fuel cells operated in mixed-feed mode. Although the mixed-reactant concept provides many opportunities to simplify fuel cell systems, few investigations have concerned the design and engineering of MRFC reactors which is the focus of the present disclosure.

For example, unconventional reactor architectures for low temperature MRFCs are presented in the surface migration cell of van Gool [11], the flow-through architecture of Priestnall [9] and the flow-by configuration of Oloman [13].

In 1965, van Gool described the surface-migration cell for MRFCs, but without experimental evaluation [11]. In this geometry, two closely spaced selective electrodes (anode and cathode) are positioned on the same side of an insulating substrate with a film electrolyte between them. In 1980, Louis et al. experimentally investigated this design and employed a supported thin-film ($3 \times 10^{-6}$ m) alumina electrolyte, along with closely spaced ($3–4 \times 10^{-4}$ m gap) supported Pt anode and $SrRuO_3$ cathode [14]. Each electrode was $5 \times 10^{-6}$ m thick with$10^{-4}$ $m^2$ geometrical surface area. With a single humidified mixed gas feed of 4 vol% $O_2$, 4 vol% $H_2$ in nitrogen, an open circuit voltage (OCV) of 0.67 V was obtained at room temperature with a peak superficial power density of $3.2 \times 10^{-2}$ W $m^{-2}$ (pressures are not mentioned in the patent [14]). They also presented the concept of a surface strip-cell geometry in which multiple pairs of electrodes are interconnected electrically in series with several of such layers connected in parallel.

In 2002, Priestnall et al., introduced a mixed-reactant flow-through fuel cell and discussed its application in a direct methanol fuel cell, SOFCs and $H_2$/proton exchange membrane (PEM) fuel cell [9]. In the flow-through architecture, the anode, cathode, and electrolyte membrane are porous, so the fuel and oxidant mixture can flow directly through the anode, membrane, and cathode in the direction of the axis and parallel to the current. Selective catalysts are coated onto the porous surfaces of the anode and cathode. Priestnall et al. have developed a seven-cell direct methanol/air mixed-reactant fuel cell stack, using a Ru based cathode and PtRu anode electrocatalysts, giving a power of about 4 W.

In 2010, a mixed-reactant flow-by fuel cell (MRFBFC) was developed by Oloman [13]. In flow-by architecture, operated in the monopolar or bipolar mode, the 2-phase fluid mixture flows generally parallel to each anode and cathode with the fluid flow orthogonal to the current. Each cell comprises an anode, a cathode, a separator situated between the anode and the cathode and a 2-phase fluid flow distributor in electronic communication with the anode and with the cathode of the adjacent unit cell. At 333 K/120 kPa(abs) with a feed of aqueous sodium formate/sodium hydroxide mixed with air this reactor gave peak superficial and volumetric power densities respectively up to 700 W $m^{-2}$ and 200 kW $m^{-3}$ [13].

Here, we introduce a cylindrical architecture for MRFCs, based on the concept of Swiss-roll electrosynthesis cells, in which a flexible sandwich of electrodes and separators is rolled around an axis to give a compact three-dimensional (3D) electrode space for the fuel cell reactions. The so-called "Swiss-roll" electrochemical reactor was developed by Robertson et al. [15,16] in 1975 for electrosynthesis of organic compounds and water treatment systems. The idea of using the Swiss-roll architecture for MRFCs was recently proposed by Oloman [13] but it has not been experimentally investigated. Therefore, the main objective of the present report is to demonstrate for the first time the concept of a Swiss-roll reactor design applied to the alkaline borohydride fuel cell.

When operated with a liquid electrolyte the Swiss-roll design has the following benefits: a) the rolled packing of the porous 3D electrode with both radial and axial flow provides an extended reaction zone with high liquid–solid mass transfer capacity, which enhances the volumetric power density of the fuel cell, b) the bipolar plates are replaced by lighter, flexible, metal screens or meshes, c) the cylindrical architecture provides a compact design for multi-polar electrode arrangement, and d) there is no need for the solid polymer membrane-electrolyte, which is a failure-prone component of PEM fuel cells [17].

In the direct borohydride/oxygen fuel cell (DBFC) the primary electrode reactions are:

$$\text{Anode}: \quad NaBH_4 + 8OH^- \rightarrow NaBO_2 + 6H_2O + 8e^- \qquad E^0_{298K} = -1.24\,V_{SHE} \tag{1}$$

$$\text{Cathode}: \quad 2O_2 + 4H_2O + 8e^- \rightarrow 8OH^- \quad E^0_{298K} = +0.40\,V_{SHE} \tag{2}$$

$$\text{Overall}: \quad NaBH_4 + 2O_2 \rightarrow NaBO_2 + 2H_2O \quad E^{cell}_{298K} = +1.64\,V \tag{3}$$

Concerning the fuel, borohydride has many advantages, including a high theoretical gravimetric energy density (9.3 kWh $kg^{-1}$ of $NaBH_4$), plus safety and stability in solid form and in concentrated alkaline solutions [18]. Also, the electro-oxidation of $BH_4^-$ has been extensively investigated over the last decade, with the goal of developing DBFCs. In experimental and theoretical studies it has been shown that the electro-oxidation of $BH_4^-$ involves a number of competitive electrocatalytic and thermocatalytic pathways, that can diminish the Faradaic equivalence from 8 to 4 electrons/mole $BH_4^-$ converted, depending on the electrocatalyst, electrode potential, temperature and $OH^-/BH_4^-$ ratio [19–24].

Apart from losses associated with the electro-oxidation mechanism, the non-Faradaic hydrolysis of $BH_4^-$, catalyzed by surfaces such as Pt and Ru, generates hydrogen that may be oxidized in-situ and/or released as a gas that interferes with transport in the anode. As first described by Lam and Gyenge [25] the problem of hydrogen gas hold up in the anode can be alleviated by the use of a 3D anode structure that promotes the electro-oxidation of hydrogen while allowing 2-phase (gas/liquid) flow to reduce the effect of gas occlusion on the cell voltage. In their work Lam et al. showed that, under otherwise similar conditions, the peak superficial power density of a DBFC increased from 800 to 1300 W $m^{-2}$ when the anode was changed from a conventional catalyst coated membrane-electrode to a 3D anode of catalyzed carbon felt. The present paper describes the first experiments with a Swiss-roll mixed-reactant fuel cell (SRMRFC) and records its proof of concept. This work used a DBFC equipped with 3D anodes and gas diffusion cathodes, operating in both the monopolar and bipolar modes on a mixed feed of aqueous alkaline sodium borohydride and oxygen gas.

Here, we report the results of short term experiments with several variables on the performance of the Swiss-roll fuel cell, plus an investigation of the reactor stability in extended operation. Finally, the figures of merit of the SRMRFC are compared to those of conventional DBFCs in which the fuel and oxidant streams are separated by an ion exchange membrane.

## 2. Experimental

Fig. 1 shows the conceptual Swiss-roll reactor components in both monopolar and bipolar mode. In broad strokes, a flexible

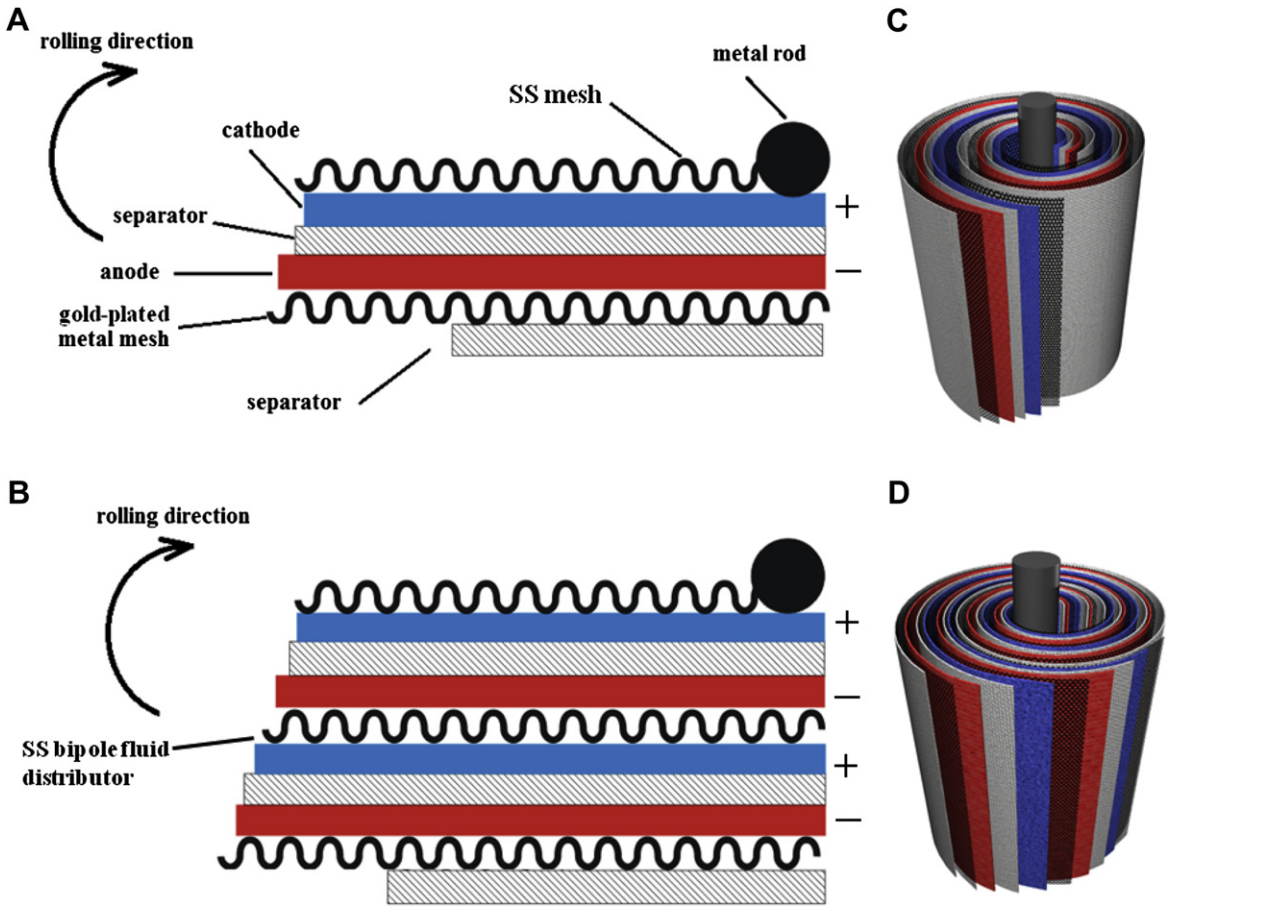


**Fig. 1.** (A) cross section of sandwich construction for monopolar Swiss-roll, (B) bipolar construction of Swiss-roll with two cells (C) schematic perspective view of the Swiss-roll electrodes after rolling in monopolar arrangement (D) bipolar arrangement for two cells. Color online.

sandwich of anode(s), cathode(s), separator(s) and metal mesh current conductor(s)/fluid distributor(s) is rolled around an electronically conductive mandrel that feeds current from/to an electrode. The outer surface of the roll exposes a counter-electrode for electronic contact with the inside of a cylindrical vessel that houses the fuel cell(s) and acts as the current collector. As in Fig. 1, this arrangement can be adapted for a single cell monopolar (Fig. 1A and C), a multi-cell bipolar (Fig. 1B and D) or a multi-cell monopolar reactor (not shown). A liquid/gas mixture of fuel and oxidant is passed longitudinally through the reactor (i.e., parallel to the central mandrel), as the two fluids move along the porous cell(s) both the anode(s) and the cathode(s) are exposed to fuel and oxidant. In this situation the performance of the reactor depends primarily on the electrocatalytic selectivity for the desired oxidation and reduction reactions and secondarily on the electrical conductivity (electronic and ionic) of the cell components.

The 3D anodes and gas diffusion cathode used in this Swiss-roll MRFC were manufactured in-house and commercially obtained, respectively. The 3D anodes were prepared by standard techniques, in which inks made of Pt/C (with 50 wt% Pt) or PtRu/C (with 20 wt% PtRu, 1:1 atom ratio) mixed with 30 wt% Nafion® (from a 5 wt% Nafion® in lower alcohols solution, Sigma–Aldrich Inc.) were sprayed by a CNC moving table equipped with an air sprayer gun onto a 0.1 m × 0.1 m woven carbon cloth (purchased from Fuel Cell Earth LLC, thickness of $3.5 \times 10^{-4}$ m). The gas-diffusion cathodes (thickness $3 \times 10^{-4}$ m) consisting of teflonated $MnO_2$/C or Ag/C catalyst layer pressed onto Au-plated Ni mesh were purchased from Gaskatel GmbH and used as is. The separator was two layers of hydrophilic microporous polypropylene (Scimat® 720/20) with thickness of about $2 \times 10^{-4}$ m, and 80% porosity.

For monopolar operation, one layer of Au-plated steel mesh (#60) was placed on the 3D anode to improve the electronic conductivity with the current collector cylindrical container surface and one layer of stainless steel screen (#40) was placed on the cathode to provide a path for fluid flow through the reactor. Catalyst loadings were $8 \times 10^{-3}$ kg m$^{-2}$ (0.8 mg cm$^{-2}$) on the anode and $5 \times 10^{-3}$ kg m$^{-2}$ (0.5 mg cm$^{-2}$) on the cathode. The total thickness of all the layers shown by Fig. 1A was about $1.8 \times 10^{-3}$ m.

A sandwich of the above components was rolled around a $9.5 \times 10^{-3}$ m (0.95 cm) diameter stainless steel rod/current collector which was in electronic contact only with the cathode. At the end of the roll the outmost exposed anode layer made a tight press fit when slid inside a $25 \times 10^{-3}$ m (25 mm) inner diameter Au-plated stainless steel cylinder, 0.10 m long by 0.03 m OD, serving as the Swiss-roll container and anode current collector. The reactor was covered with a $10^{-2}$ m (1 cm) thick layer of insulation.

For dual-cell bipolar operation, the 3D Pt/C anode and gas-diffusion $MnO_2$ cathode was employed. As shown in Fig. 1B a bipole fluid distributor (stainless steel mesh #40) is placed between the cathode of the first cell and the anode of the adjacent cell to provide the necessary electrical conductivity between two cells. A sandwich of dual cell is rolled around the current collector and slid inside of the Swiss-roll container and anode current collector.

As shown in the flow sheet in Fig. 2, the cylindrical reactor (fuel cell) was supplied with a downward two-phase flow of continuous metered flows of alkaline sodium borohydride solution and oxygen gas. The liquid feed was aqueous 1 M $NaBH_4$ + 2 M NaOH and pumped by a Masterflex® peristaltic pump. The oxidant was oxygen gas (99.99 vol. %, Praxiar) and monitored by a Fideris™ fuel cell test station. The 2-phase reactant feed mixture was preheated to a controlled temperature and the pressure (P) and temperature (T) across the reactor measured by digital pressure gauges and thermocouples, respectively. The gas feed was fixed in all experiments at 10 standard liter per minute (SLPM) while the liquid flow ranged from 5 to 15 mL $min^{-1}$.The feed temperature and pressure were kept at 323 K and 105 kPa(abs) while the pressure and temperature drop across the fuel cell elements were respectively about 2 kPa and 6 K.

Experimental runs consisted of fixing the process conditions and measuring the fuel cell polarization curve. In all polarization experiments, except the tests for stability and liquid flow effects in the bipolar mode, a new anode and cathode was used. For the study of fuel cell durability, both 3 h continuous operation and multi-day shut-down/start-up tests were carried out. Before shutting it down the reactor was washed with a mixed feed of deionized water and $N_2$ gas for 15 min at 323 K at the 10 mL $min^{-1}$ of liquid and 10 SLPM of $N_2$ then left to cool overnight. On the next day, the reactor was started up with fresh feed to investigate the stability of the reactor performance after several shut downs and start ups.

Regarding calculation of figures of merits, current drawn from reactor is divided by geometrical surface area of electrodes ($2 \times 10^{-3}$ $m^2$) to calculate the superficial current density (in A $m^{-2}$). The superficial current densities are multiplied by the total voltage of the cell(s) to calculate superficial power densities. For calculation of volumetric power densities, current drawn from the reactor is divided by the physical volume of the Swiss-roll occupied between the middle rod and reactor vessel to calculate the volumetric current density (in kA $m^{-3}$). The volumetric current densities are multiplied by total voltage of the cell(s) to calculate volumetric power densities (kW $m^{-3}$).

## 3. Results and discussion

Fig. 3 shows polarization curves for the Swiss-roll MRFC comparing Pt/C with PtRu/C as anode electrocatalysts (Fig. 3A) and Ag/C with $MnO_2$/C as cathode electrocatalysts (Fig. 3B). The electrocatalytic selectivity is paramount for the operation of any mixed-reactant system. In this regard, Chatenet et al. reported that $MnO_2$ was selective toward the oxygen reduction reaction (ORR) in the presence of $BH_4^-$ [26]. Moreover, the different hydrophobic-hydrophilic balance of the anode and cathode, namely, the hydrophobic gas-diffusion cathode and the hydrophilic 3D anode, probably helps to separate the two electrode reactions and suppress mixed potentials.

Comparing Pt/C and PtRu/C anode electrocatalysts coupled with $MnO_2$/C (Fig. 3A), Pt/C gave superior results over the entire polarization curve, with a peak superficial power density of 640 W $m^{-2}$ whereas under the same conditions PtRu/C generated only 280 W $m^{-2}$. From replicated runs with single cells using Pt/C anode and MnO2/C cathode the standard error of the mean peak superficial power density was 11 W $m^{-2}$. The open-circuit voltage (OCV) was 0.80 V for Pt/C and 0.60 V for PtRu/C. Based on the standard cell potential corresponding to the direct oxidation of $BH_4^-$ (i.e., 1.64 V at 298 K, Eq. (3)) a higher OCV might be expected. The loss of OCV is presumably due to the $H_2$ evolution and oxidation in the anode discussed in the previous sections combined with mixed potentials on the electrodes from fuel ($BH_4^-$ and $H_2$) oxidation and $O_2$ reduction. In particular, the development of a mixed potential on the anode cannot be prevented because dissolved $O_2$ will always reach the catalytic sites in the 3D electrode.

Regarding the hydrogen evolution, Ru is a more active catalyst than Pt for the $BH_4^-$ hydrolysis [25]:

$$BH_{4\ (aq)}^- + 2H_2O \rightarrow 4H_2 + BO_{2\ (aq)}^- \quad (4)$$

Therefore, the anodic reaction will be a combination of direct borohydride oxidation (Eq. (1)) and hydrogen oxidation according to Eq. (5):

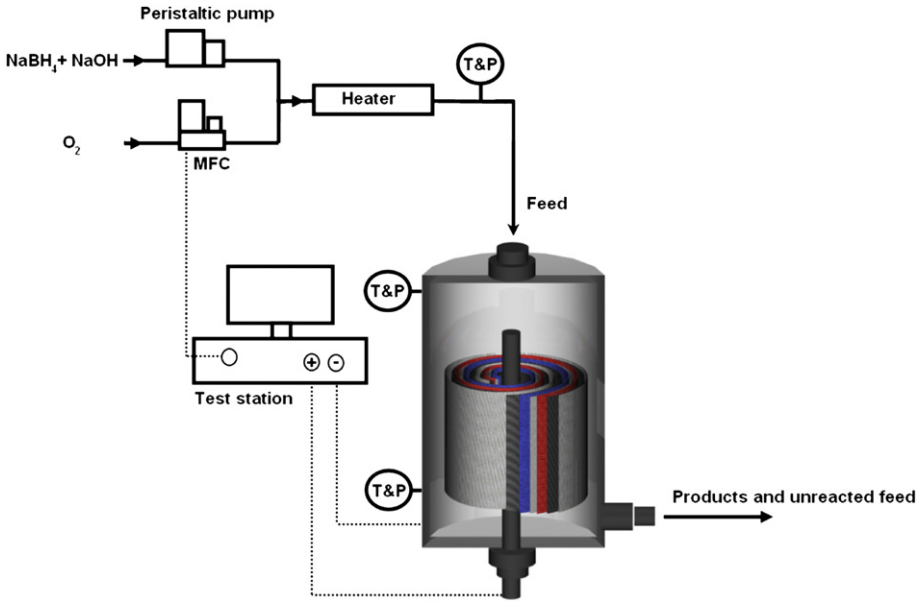


**Fig. 2.** Experimental apparatus of Swiss-roll mixed-reactant fuel cell. Color online.

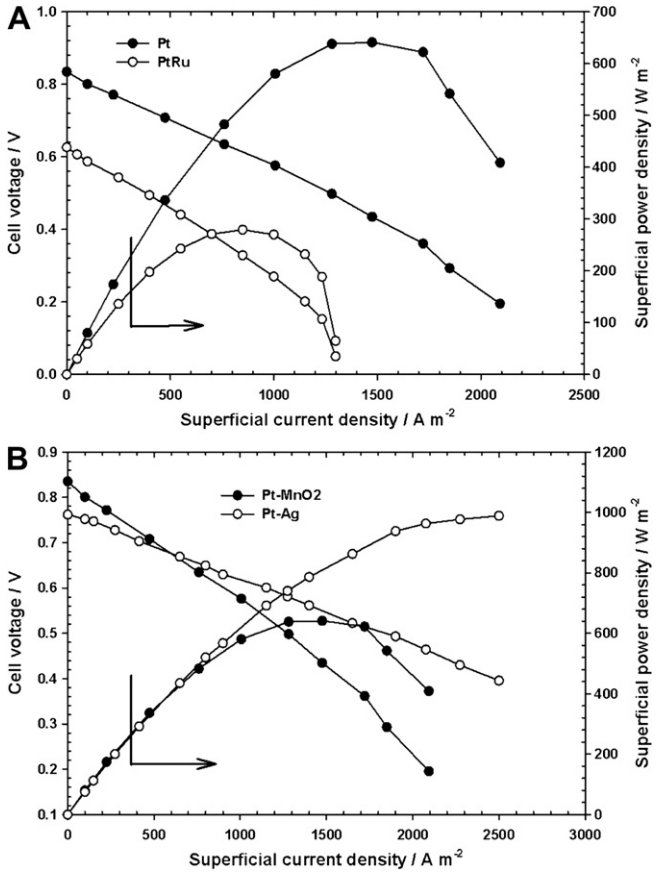


**Fig. 3.** Effect of electrocatalysts on the Swiss-roll single-cell monopolar MRFC (A) anode (Pt/C or PtRu/C) – $MnO_2$/C cathode (B) Pt/C anode – cathode ($MnO_2$/C or Ag/C); feed: 1 M $NaBH_4$+2 M NaOH (8 mL/min), $O_2$ (10 SL/min), 323 K, 105 kPa(abs).

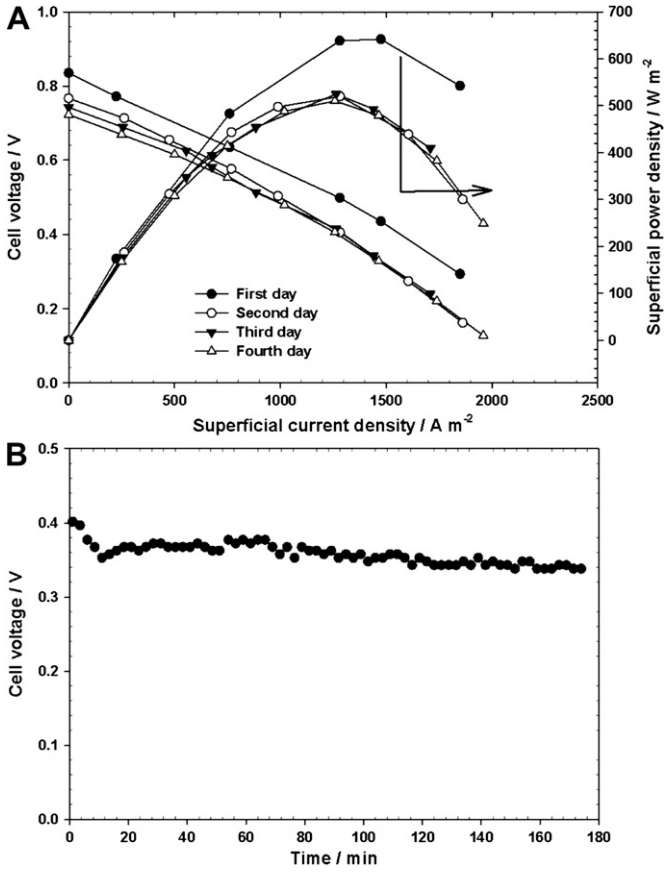


**Fig. 4.** Stability of the Swiss-roll single-cell monopolar MRFC. (A) repeated polarization curves after 24 h of idle time, B) galvanostatic stability at 1500 A $m^{-2}$ in the first day of operation. Pt/C anode, $MnO_2$/C cathode. Other conditions as in Fig. 3.

$$H_2 + 2OH^- \rightarrow 2H_2O + 2e^-_{(aq)} \quad E^0_{298K} = -0.83\ V_{SHE} \tag{5}$$

Furthermore, at superficial current densities above 1100 A $m^{-2}$ the higher rate of $H_2$ evolution on PtRu causes mass transfer limitation for the $BH_4^-$, which is manifested in the corresponding sharp drop of the cell voltage (Fig. 3A).

For the cathode, two electrocatalysts were investigated: Ag/C and $MnO_2$/C (Fig. 3B). Both are good ORR electrocatalysts in alkaline media [27–29]. In contrast to $MnO_2$, Ag is also a good electrocatalyst for borohydride oxidation [30] and would not seem acceptable in the cathode of a borohydride/oxygen MRFC. Fig. 3B, compares the performance of Pt/C–$MnO_2$/C and Pt/C–Ag/C anode–cathode electrocatalyst pairs. The open circuit voltage with the Ag/C is slightly lower than that with the $MnO_2$/C cathode i.e., 0.75 V vs. 0.80 V, confirming a higher mixed potential on Ag. However, at superficial current densities above 500 A $m^{-2}$ the cell voltage was significantly higher with the Ag/C cathode, reaching a peak superficial power density of 1000 W $m^{-2}$, compared to 640 W $m^{-2}$ for $MnO_2$. To the knowledge of the authors, 640 W $m^{-2}$ is higher than any peak power density reported in previous work for low temperature (up to 400 K) mixed-reactant fuel cells. The differences between the two cathodes of Fig. 3B could be due to a lower activation polarization and/or a higher electronic conductivity of Ag/C compared to $MnO_2$/C in the gas-diffusion electrode. Since $MnO_2$ has an initial fixed cost advantage over Ag, the $MnO_2$/C gas diffusion cathode was used with the 3D Pt/C carbon cloth anode in our subsequent studies of temporal stability and bipolar cells.

Concerning the fuel cell temporal stability, Fig. 4A depicts the performance of the Swiss-roll MRFC over a four-day period involving shut down/start ups. The OCV and peak superficial power density for the first day of operation were respectively 0.85 V and 640 W $m^{-2}$ On the second day of operation, after one shut down and idle time of some 24 h the OCV dropped to about 0.77 V and the peak superficial power density decreased to

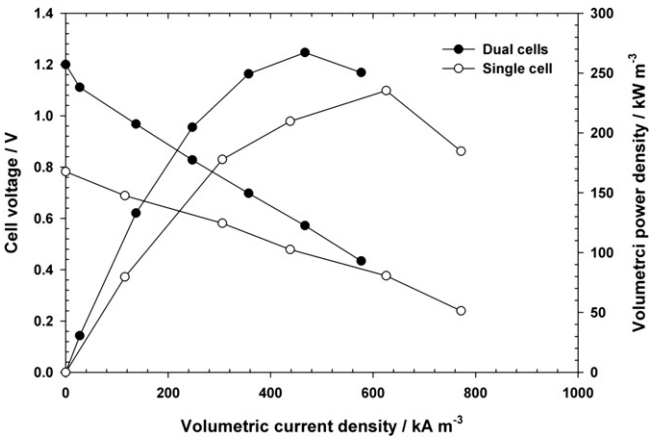


**Fig. 5.** Comparison of single-cell monopolar and dual-cell bipolar operation of the Swiss-roll MRFC. Conditions as in Fig. 3B.

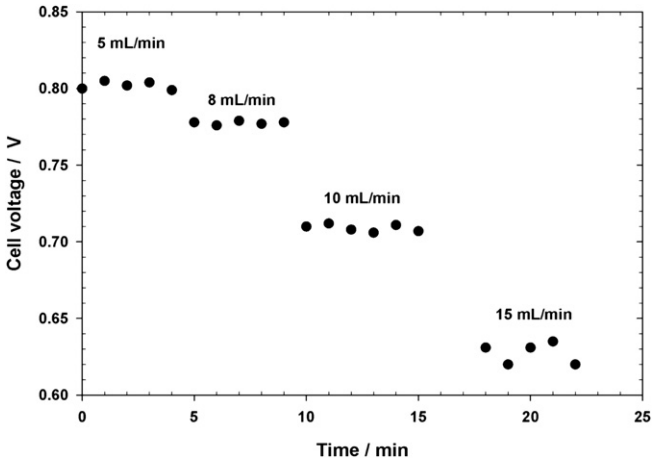


**Fig. 6.** Effect of liquid flow in a dual-cell bipolar Swiss-roll MRFC. Constant current density of 1500 A $m^{-2}$, liquid flow rate changed every 5 min, oxygen gas flow 10 SL/min, 323 K, 105 kPa(abs).

500 W $m^{-2}$. This performance loss may be attributed to NaOH crystallization and/or carbonation, loss of hydrophobicity in the gas-diffusion cathode and possibly electrocatalyst poisoning. However, after the second day shut down there was no significant performance drop when the fuel cell was restarted in days three and four. Fig. 3B shows stability of the Swiss-roll MRFC over a 3 h continuous operation at a constant current density of 1500 A $m^{-2}$ during the second day of these tests (see discussion for Fig. 4A). After the initial decline of some 0.05 V the additional voltage drop over 3 h was about 0.03 V. These promising preliminary stability data warrant further and more detailed durability investigations.

Next we demonstrate the bipolar operation, as a first step in developing a compact cylindrical Swiss-roll stack composed of N-cells in series. Fig. 5 shows the polarization curve of the Swiss-roll MRFC composed of two cells in series. The open circuit voltage was 1.2 V, while the OCV of a single cell was 0.8 V. The fact that the dual cell OCV is not near two times that of a single cell can be explained by the establishment of shunt currents, which are a common occurrence in multi-polar electrochemical reactors when there is an ionically conductive pathway between cells [31]. In bipolar fuel cells shunt current lowers both the OCV and the operating voltage. Thus the peak volumetric power densities for single cell and dual cell Pt/C 3D anode-$MnO_2$/C gas diffusion cathode Swiss-roll MRFC were 237 kW $m^{-3}$ and 267 kW $m^{-3}$, respectively.

Fig. 6 illustrates a critical feature of the bipolar Swiss-roll MRFC respecting fluid flow through the cells. In this reactor, the bipolar plates of a conventional fuel cell are replaced by coarse metal screens that form the main passages for flow of the two-phase fuel-oxidant mixture through each cell, while providing electronic contact between adjacent cells. The effectiveness of this design depends on maintaining a high gas to liquid hold up ratio, and consequent low effective ionic conductivity, in the bipole fluid distributors. As shown in Fig. 1 and outlined above, ionic conduction in the bipoles allows shunt currents that essentially by-pass the Faradaic processes and compromise the reactor performance. This result is clear in Fig. 6, where the bipolar reactor voltage at 1500 A $m^{-2}$ goes from about 0.8 to 0.6 V as the gas to liquid flow ratio drops from around 2000 to 700. Such fluid dynamic effects are important in scaling up the Swiss-roll MRFC.

Finally, Table 1 compares the peak superficial power densities for various PEM DBFCs reported in the literature with those from the Swiss-roll MRFC. Volumetric power densities are not available from the source documents. The peak superficial power densities obtained for the Swiss-roll cell design compare favorably with those from the conventional PEM DBFC operating under similar conditions of temperature and pressure. Apart from the work using anodes with high palladium loads and cathodes with non-Pt cathode catalysts and air oxidant the power density from the Swiss-roll was exceeded only by PEM DBFCs with a higher Pt cathode loading and/or higher temperature and or $O_2$ pressure than those used in the Swiss-roll MRFC.

**Table 1**
Performance comparison of conventional DBFCs (for a review please see [32]) and the Swiss-roll MRFC.

| Anode (load/mg $cm^{-2}$) | Cathode (load/mg $cm^{-2}$) | Separator | Oxidant | T/$PO_2$ K/kPa | Peak superficial power density W $m^{-2}$ | Ref. |
|---|---|---|---|---|---|---|
| Au/C (2) | Pd/C (2) | Nafion®–117 | $O_2$ | 358/101 | 656 | [33] |
| Os (1) | Pt black (4) | Nafion®–117 | $O_2$ | 333/348 | 690 | [34] |
| Pt/C (1) | Pt/C (1) | Nafion®–212 | $O_2$ | 333/200 | 1000 | [35] |
| PtRu (1) | Pt black (4) | Nafion®–117 | $O_2$ | 333/348 | 1300 | [25] |
| Ni/C (1) | Pt/C (1) | Nafion®–212 | $O_2$ | 333/200 | 1500 | [35] |
| Ni/C (2) | Pt/C (2) | Nafion®–117 | $O_2$ | 358/101 | 405 | [33] |
| Pd/C (2) | Pt/C (2) | Nafion®–117 | $O_2$ | 358/101 | 896 | [33] |
| Pt/C (2) | Pt/C (2) | Nafion®–117 | $O_2$ | 358/101 | 513 | [33] |
| Ni–Pt/C (1) | Pt/C (1) | Nafion®–212 | $O_2$ | 333/200 | 2210 | [35] |
| Pt–Ru/C (1) | Pt/C (1) | Morgan® ADP | $O_2$ | 333/101 | 1490 | [36] |
| Ag/C (2) | Pt/C (2) | Nafion®–117 | $O_2$ | 358/101 | 436 | [33] |
| Ag/Ti (2) | Pt/C (2) | Nafion®–117 | $O_2$ | 358/101 | 500 | [37] |
| Au/C (2) | Ag/C (2) | Nafion®–117 | $O_2$ | 358/101 | 328 | [33] |
| Au/C (2) | Ni/C (2) | Nafion®–117 | $O_2$ | 358/101 | 354 | [33] |
| Au/C (2) | Pt/C (2) | Nafion®–117 | $O_2$ | 358/101 | 722 | [38] |
| Au/C (2) | FeTMPP (2) | Nafion®–117 | $O_2$ | 358/200 | 653 | [39] |
| Au/Ti (2) | Pt/C (2) | Nafion®–117 | $O_2$ | 358/101 | 814 | [37] |
| Ni powder (167) | Pt/C (1) | Nafion®–212 | Air | 298/101 | 400 | [40] |
| Pd/C (1.08) | Pt/C (0.3) | Nafion®–117 | Air | 298/NA | 194 | [41] |
| Pt/C (1.3) | Non-Pt/Ni mesh (NA) | Morgan® ADP | Air | 298/101 | 2000 | [42] |
| Ni + Pd/C (20) | Pt/C (1) | Nafion®–112 | Air | 323/NA | 2500 | [43] |
| Pt–Ni/C | Non-Pt/Ni mesh (NA) | Morgan® ADP | Air | 293/NA | 1150 | [42] |
| Pt/C (0.8) | Ag/C (0.5) | Scimat® (770/20) | $O_2$ | 323/105 | 1000 | This work |
| PtRu/C (0.8) | $MnO_2$/C (0.5) | Scimat® (770/20) | $O_2$ | 323/105 | 280 | This work |
| Pt/C (0.8) | $MnO_2$/C (0.5) | Scimat® (770/20) | $O_2$ | 323/105 | 640 | This work |

## 4. Conclusion

This work demonstrated for the first time the operation of a direct borohdyride fuel cell in mixed-reactant mode, using the Swiss-roll cell architecture. Superficial peak power densities of up to 1000 W $m^{-2}$ were obtained with very promising durability that warrant further engineering improvements and optimization for a compact, light-weight, stack development, which is the focus of our ongoing work. The product is an alkaline $NaBO_2$ solution. The solubility of $NaBO_2$ in 2 M NaOH is about 10.5 wt% [44]. The recycling of $NaBO_2$ to $NaBH_4$ either thermocatalytically or electrochemically [45], is not feasible at present. Unequivocally, if the recycling of $NaBO_2$ becomes a reality it will increase the attractiveness of this technology.

The experiments presented here used pure $O_2$ on the cathode but in our most recent experiments we use air with very good preliminary results that will be presented in future publications. Alkaline metal-air fuel cell technologies such as Zn-air or Mg-air that could be considered competitors for the borohydride-air system have their own limitations such as lower gravimetric energy densities, parasitic negative difference effect (especially for Mg) and batch operation with anode consumption by electrodissolution. Carbonation of the electrolyte could be an issue for any alkaline fuel cell and battery technology. However, it has been successfully addressed in the literature by stripping $CO_2$ from the air feed [46] and/or modifying the porous electrode structure creating larger pores that are less prone to clogging. The three-dimensional anode used in this work has larger pores compared to conventional gas diffusion electrodes therefore, anode fouling is less likely.

Lastly, it is important to emphasize the mixed reactant Swiss-roll reactor design is not limited to either the borohydride-oxygen system or to alkaline fuel cells in general. It could be applied for a variety of systems in acid media as well, such as methanol-transition metal redox couple (e.g., Fe(III)/Fe(II) [47] or hydrogen-transition metal redox couple fuel cells [48].

## Acknowledgments

The authors gratefully acknowledge the financial assistance of the Natural Sciences and Engineering Research Council of Canada (NSERC) through the Discovery and Discovery Accelerator Grant programs, as well as the support of the University of British Columbia and the associated Clean Energy Research Centre.

## References

[1] A.K. Shukla, R.K. Raman, K. Scott, Fuel Cells 5 (2005) 436–447.
[2] D.J.L. Brett, N.P. Brandon, J. Fuel Cell Sci. Technol. 4 (2007) 29–44.
[3] R. Kothandaraman, W. Deng, M. Sorkin, A. Kaufman, H.F. Gibbard, S.C. Barton, J. Electrochem. Soc. 155 (2008) B865–B868.
[4] D. Papageorgopoulos, F. Liu, O. Conrad, Electrochim. Acta 52 (2007) 4982–4986.
[5] H. Meng, M. Wu, X.X. Hu, M. Nie, Z.D. Wei, P.K. Shen, Fuel Cells 6 (2006) 447–450.
[6] R. Zeng, P.K. Shen, J. Power Sources 170 (2007) 286–290.
[7] A.B. Ilicic, D.P. Wilkinson, K. Fatih, J. Electrochem. Soc. 157 (2010) B529–B535.
[8] S.C. Barton, T. Patterson, E. Wang, T.F. Fuller, A.C. West, J. Power Sources 96 (2001) 329–336.
[9] M.A. Priestnall, V.P. Kotzeva, D.J. Fish, E.M. Nilsson, J. Power Sources 106 (2002) 21–30.
[10] C.K. Dyer, Nature 343 (1990) 547–548.
[11] W. van Gool, Philips Res. Rep. 20 (1965) 81–93.
[12] M. Yano, A. Tomita, M. Sano, T. . Hibino, Solid State Ionics 177 (2007) 3351–3359.
[13] C.W. Oloman. U.S. Patent Application 2011/0171555A1.
[14] G. A. Louis, J. M. Lee, D. L. Maricle, J. C. Trocciola. U.S. Patent, 1981; 4, 248, 941.
[15] P.M. Robertson, N. Ibl, J. Appl. Electrochem. 7 (1977) 323–330.
[16] P.M. Robertson, Electrochim. Acta 22 (1977) 411–419.
[17] D.P. Wilkindson, J. St-Pierre, in: W. Vielstich, A. Lamm, H.A. Gasteiger (Eds.), Handbook of Fuel Cells: Fundamentals, Technology, Applications, first ed. Wiley, Chichester, England, 2003, pp. 611–621.
[18] D.M.F. Santos, C.A.C. Sequeira, Renewable Sustainable Energy Rev. 15 (2011) 3980–4001.
[19] E. Gyenge, M. Atwan, D. Northwood, J. Electrochem. Soc. 153 (2006) A150–A158.
[20] D.A. Finkelstein, N.D. Mota, J.L. Cohen, H.D. Abruña, J. Phys. Chem. C 113 (2009) 19700–19712.
[21] B. Molina Concha, M. Chatenet, E.A. Ticianelli, F.H.B. Lima, J. Phys. Chem. C 115 (2011) 12439–12447.
[22] V.W.S. Lam, D.C.W. Kannangara, A. Alfantazi, E.L. Gyenge, J. Phys. Chem. C 115 (2011) 2727–2737.
[23] M.C.S. Escaño, E. Gyenge, R.L. Arevalo, H. Kasai, J. Phys. Chem. C 115 (2011) 19883–19889.
[24] G. Rostamikia, M.J. Janik, Energy Environ. Sci. 3 (2010) 1262.
[25] V.W.S. Lam, A. Alfantazi, E.L. Gyenge, J. App. Electrochem. 39 (2009) 1763–1770.
[26] M. Chatenet, F. Micoud, I. Roche, E. Chainet, J. Vondrák, Electrochimica Acta 51 (2006) 5452–5458.
[27] I. Roche, E. Chainet, M. Chatenet, J. Vondrak, J. Phys. Chem. C 111 (2007) 1434–1443.
[28] D. Sepa, M. Vojnovi, A. Damjanovict, Electrochim. Acta 15 (1970) 1355–1366.
[29] E.L. Gyenge, J.F. Drillet, J. Electrochem. Soc. 159 (2012) F23–F34.
[30] M.H. Atwan, D.O. Northwood, E.L. Gyenge, Int. J. Hydrogen Energy 32 (2007) 3116–3125.
[31] A.T. Kuhn, J.S. Booth, J. Appl. Electrochem 10 (1980) 233–237.
[32] J. Ma, N.A. Choudhury, Y. Sahai, Renewable Sustainable Energy Rev. 14 (2010) 183–199.
[33] H. Cheng, K. Scott, K. Lovell, Fuel Cells 6 (2006) 367–375.
[34] V.W.S. Lam, E.L. Gyenge, J. Electrochem. Soc. 155 (2008) B1155.
[35] X. Geng, H. Zhang, W. Ye, Y. Ma, H. Zhong, J. Power Sources 185 (2008) 627–632.
[36] N. Duteanu, G. Vlachogiannopoulos, M.R. Shivhare, E.H. Yu, K. Scott, J. Appl. Electrochem 37 (2007) 1085–1091.
[37] H. Cheng, K. Scott, J. Appl. Electrochem 36 (2006) 1361–1366.
[38] H. Cheng, K. Scott, J. Power Sources 160 (2006) 407–412.
[39] H. Cheng, K. Scott, J. Electroanal. Chem. 596 (2006) 117–123.
[40] B.H. Liu, Z.P. Li, K. Arai, S. Suda, Electrochim. Acta 50 (2005) 3719–3725.
[41] C. Celik, F.G.B. San, H.I. Sarac, J. Power Sources 185 (2008) 197–201.
[42] R. Jamard, A. Latour, J. Salomon, P. Capron, A. Martinent-Beaumont, J. Power Sources 176 (2008) 287–292.
[43] Z.P. Li, B.H. Liu, J.K. Zhu, S. Suda, J. Power Sources 163 (2006) 555–559.
[44] C. Cloutier, A. Alfantazi, E. Gyenge, J. Fuel Cell Sci. Tech 4 (2007) 88–98.
[45] E. Gyenge, C. Oloman, J. Appl. Electrochem. 28 (1998) 1147–1151.
[46] J.-F. Drillet, F. Holzer, T. Kallis, S. Müller, V.M. Schmidt, Phys. Chem. Chem. Phys. 3 (2011) 368–371.
[47] A. Ilicic, M.S. Dara, D.P. Wilkinson, K. Fatih, J. Appl. Electrochem. 40 (2010) 2125–2133.
[48] K. Fatih, D.P. Wilkinson, F. Moraw, A. Ilicic, F. Girard, Electrochem. Solid-St Lett. 11 (2008) B11–B15.